blood®
Regular Article

MYELOID NEOPLASIA

Loss of a 7q gene, *CUX1*, disrupts epigenetically driven DNA repair and drives therapy-related myeloid neoplasms

Molly K. Imgruet,[1,2] Julian Lutze,[3,4] Ningfei An,[1] Bonnie Hu,[1] Saira Khan,[1] Jeffrey Kurkewich,[1] Tanner C. Martinez,[1,2] Donald Wolfgeher,[3] Sandeep K. Gurbuxani,[1,5] Stephen J. Kron,[3,4,5] and Megan E. McNerney[1,4,5,6]

[1]Department of Pathology, [2]Medical Scientist Training Program, [3]Department of Molecular Genetics and Cell Biology, [4]Committee on Cancer Biology, [5]The University of Chicago Medicine Comprehensive Cancer Center, and [6]Section of Pediatric Hematology/Oncology and Stem Cell Transplantation, Department of Pediatrics, The University of Chicago, Chicago, IL

KEY POINTS

- CUX1 recruits the histone methyltransferase EHMT2 to sites of DNA damage to promote γH2AX focus formation and DNA damage repair.
- Loss of CUX1 drives clonal hematopoiesis following chemotherapy and predisposes mice to an aggressive t-MN.

Therapy-related myeloid neoplasms (t-MNs) are high-risk late effects with poorly understood pathogenesis in cancer survivors. It has been postulated that, in some cases, hematopoietic stem and progenitor cells (HSPCs) harboring mutations are selected for by cytotoxic exposures and transform. Here, we evaluate this model in the context of deficiency of CUX1, a transcription factor encoded on chromosome 7q and deleted in half of t-MN cases. We report that CUX1 has a critical early role in the DNA repair process in HSPCs. Mechanistically, CUX1 recruits the histone methyltransferase EHMT2 to DNA breaks to promote downstream H3K9 and H3K27 methylation, phosphorylated ATM retention, subsequent γH2AX focus formation and propagation, and, ultimately, 53BP1 recruitment. Despite significant unrepaired DNA damage sustained in CUX1-deficient murine HSPCs after cytotoxic exposures, they continue to proliferate and expand, mimicking clonal hematopoiesis in patients postchemotherapy. As a consequence, preexisting CUX1 deficiency predisposes mice to highly penetrant and rapidly fatal therapy-related erythroleukemias. These findings establish the importance of epigenetic regulation of HSPC DNA repair and position CUX1 as a gatekeeper in myeloid transformation.

Introduction

A devastating sequela of the use of chemotherapy and/or irradiation is the development of a secondary malignancy. Therapy-related myeloid neoplasms (t-MNs) are blood cancers that develop as a consequence of genotoxic treatments for several conditions, most commonly cancer. t-MNs are associated with high-risk karyotypes, chemoresistance,[1] and poor survival.[2] As cancer survivors are a growing population,[3] the incidence of t-MN is expected to rise. Treatment and prevention of this long-term side effect is of increasing importance.

Historically, t-MN was thought to be primarily driven by exposure to DNA-damaging agents and subsequent mutations in hematopoietic stem and progenitor cells (HSPCs). More recently, the etiology of this disease has been appreciated to also include inherited genetic predisposition, therapy-induced changes in the bone marrow microenvironment, and the selection of preexisting, somatically mutated hematopoietic stem cells (HSCs).[4] The latter phenomenon, termed clonal hematopoiesis of indeterminate potential (CHIP), is linked to an elevated risk of t-MNs.[5,6] This association evokes a model wherein clonal populations harboring certain mutations have a fitness advantage in the setting of chemotherapy and/or irradiation, outcompete wild-type counterparts, and transform. Somatic mutations have been found across a variety of genes and in a high percentage of healthy individuals,[7] yet only some progress to either de novo or therapy-related malignancy.[8] Mutations in epigenetic regulators, such as *DNMT3A* and *TET2*, are frequent in CHIP in healthy older adults.[9,10] In contrast, DNA damage response (DDR) genes, such as *TP53*, are more commonly mutated in CHIP following cytotoxic therapy.[11] Despite these patterns, which CHIP mutations confer the highest risk of transformation for either therapy-related or de novo disease is incompletely understood.

Monosomy 7 and del(7q) are adverse-risk cytogenetic abnormalities found in a variety of hematopoietic disorders including pediatric and adult myelodysplastic syndrome (MDS) and acute myeloid leukemia (AML).[12-15] Most striking is the prevalence of −7/del(7q) in t-MNs, where it occurs in up to 49% of cases, and particularly those associated with exposure to alkylating agents.[1] −7 and del(7q) are detected in CHIP and can be initiating events in transformation.[16-19] However, the pathogenesis of −7/del(7q) in t-MNs remains unclear.

We identified *CUX1* as a haploinsufficient tumor-suppressor gene encoded on 7q22.1.[20,21] In addition to *CUX1* loss through −7/del(7q), *CUX1*-inactivating mutations occur in CHIP, myeloid malignancies, and solid tumors.[5,9,22-25] Furthermore, *CUX1* mutations independently carry a poor prognosis in myeloid

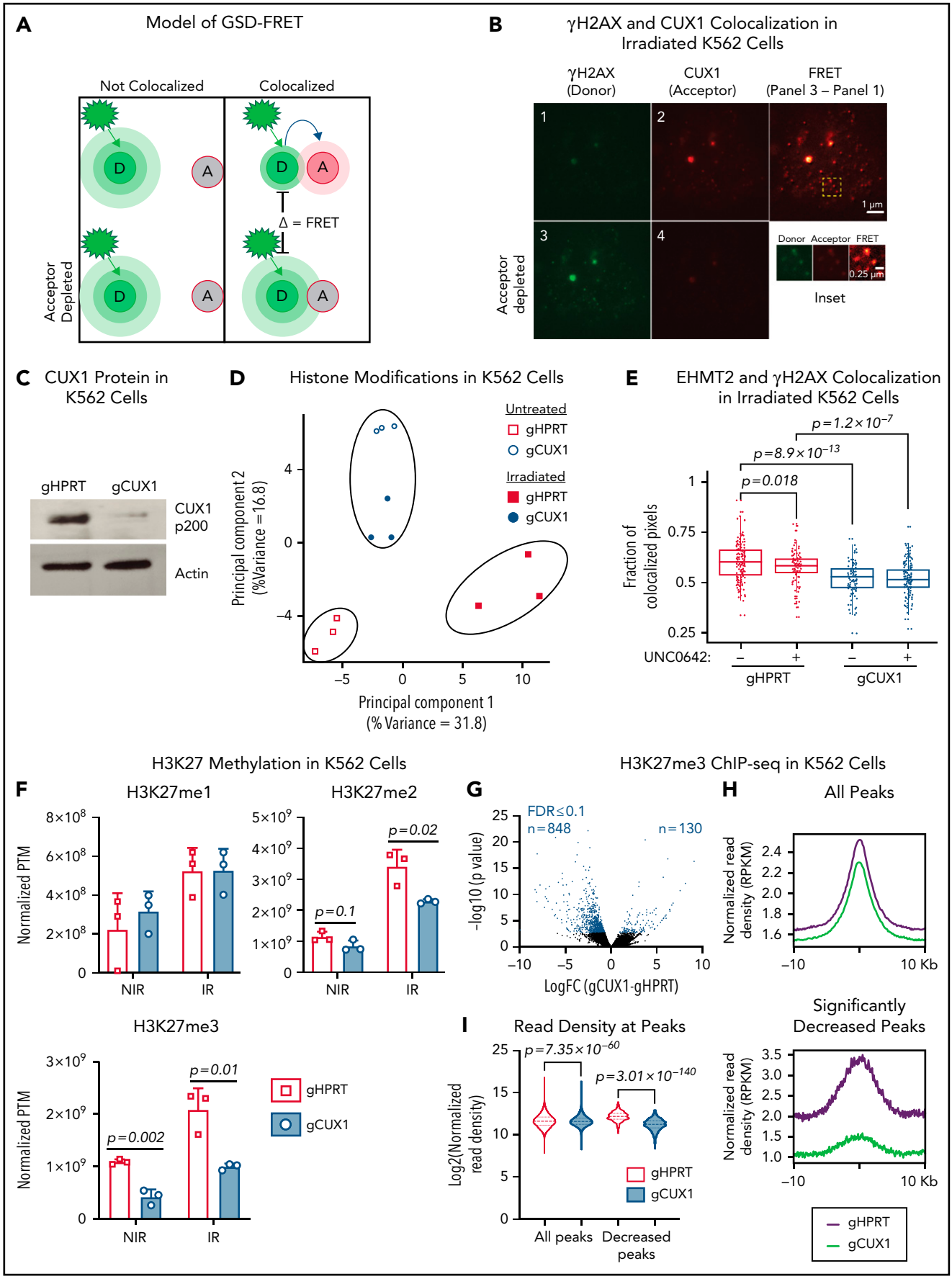

Figure 1.

malignancies.[25-27] CUX1 is a nonclustered HOX family transcription factor that is ubiquitously expressed and regulates critical cellular processes such as proliferation and differentiation in disparate cell types.[20,28,29] To identify the role of CUX1 in hematopoiesis, we generated 2 doxycycline-inducible, short hairpin RNA (shRNA)-based transgenic CUX1-knockdown mouse lines. CUX1-knockdown mice develop MDS and MDS/myeloproliferative neoplasm (MPN).[20] Thus, loss of this single 7q gene is sufficient to cause de novo myeloid malignancies.

In this study, we report that CUX1-knockdown mice are profoundly predisposed to alkylating agent–induced t-MNs. Mechanistically, we reveal a novel role for CUX1 in epigenetic regulation of the local DDR. Correspondingly, insufficient CUX1 disrupts DNA damage–induced epigenetic changes, leading to attenuated DNA damage focus formation and sustained DNA breaks. Our work illustrates the paradigm that preexisting somatic mutations are selected for and transform post–alkylating agent exposure and underscores the influence of defective DDR in t-MN susceptibility.

Methods

Colocalization

Colocalization was determined using code written to implement the intensity correlation analysis method developed by Li et al.[30,31] Regions of interest corresponding to individual nuclei were segmented, cropped, and saved as intensity matrices. Corresponding matrices were transformed into colocalization scores. Pixels were considered to be colocalized if the intensity in a given pixel was above the mean intensity for an image in both channels. We reported the fraction of pixels within a given nuclear region of interest that was colocalized. This method is insensitive both to the amount of staining present in an image and variations in intensity between cells or regions of an image.

DDR treatments

The EHMT1 inhibitor UNC0642 (Selleck Chemicals) was used at a concentration of 10 nM in culture for the indicated length of time. Irradiation was induced by exposure to a ^{60}Co source. Dosage rates varied between 10.5 and 9.1 cGy/s. Nonirradiated (NIR) samples were mock irradiated. *N*-ethyl-*N*-nitrosourea (ENU; Sigma) was dissolved in 10% ethanol (95%) and 90% phosphate-buffered saline and administered intraperitoneally (100 mg/kg). Etoposide (Sigma) was dissolved in dimethyl sulfoxide. Daunorubicin (Selleck Chemicals) was dissolved in water. Cisplatin was purchased from The University of Chicago pharmacy.

Bone marrow transplants

For competitive bone marrow transplants, 2×10^6 red blood cell (RBC)-depleted cells were transplanted, with 20% *Renilla* luciferase (Ren), Cux1^{mid}, or Cux1^{low} cells and 80% wild-type competitor (C57BL/6, CD45.1) transplanted retro-orbitally into lethally irradiated (γ-irradiation, 8.5 Gy) C57BL/6 (CD45.1) recipient mice. Doxycycline (Dox) was given after transplant, and ENU was administered (100 mg/kg) intraperitoneally at week 5, with a second dose following 9 days later.

Results

CUX1 loss impairs EHMT2 recruitment to DNA breaks and disrupts DNA damage–induced histone methylation

CUX1 has been shown to accumulate at sites of DNA damage in nonhematopoietic cells,[32] suggesting a direct and localized effect on DNA repair. We first verified this recruitment 1 hour postirradiation in MCF7 human breast cancer cells using ground state depletion (GSD) superresolution imaging of CUX1 colocalization with γH2AX, a marker of double-strand breaks (DSBs)[33] (supplemental Figure 1A, available on the *Blood* Web site). We next determined whether this finding extended to hematopoietic cells using human K562 chronic myelogenous leukemia cells. We used GSD imaging and Förster resonance energy transfer (FRET) between γH2AX (donor) and CUX1 (acceptor) fluorophores (Figure 1A). One hour postirradiation, FRET was observed (Figure 1B), indicating that CUX1 is rapidly recruited to sites of DNA damage in hematopoietic cells.

We next assessed the transcriptional role for CUX1 in the DDR. It has been reported that CUX1 transcriptionally upregulates expression of DDR genes, including *ATM* and *ATR*, in MCF7 cells and mouse embryonic fibroblasts.[34] However, we did not observe decreased *ATM* or *ATR* transcripts in RNA-sequencing (RNA-seq) data from either K562 cells or human CD34$^+$ HSPCs after

Figure 1. CUX1 loss impairs EHMT2 recruitment to DNA breaks and disrupts DNA damage–induced histone methylation changes. (A) Model of GSD-FRET. Target proteins are identified with antibodies tagged with either a donor (D) or acceptor (A) fluorophore. An image is taken using the donor excitation maxima. If the donor fluorophore is not near an acceptor fluorophore, the donor will emit all energy at the donor emission wavelength (left panel, top). If the donor is colocalizing with the acceptor fluorophore, some of the donor emission energy will be transferred to the acceptor, in proportion to the proximity to the acceptor (right panel, top). The samples are then bleached at the acceptor wavelength, and the bleached acceptors are no longer able to absorb energy. The samples are then reimaged at the donor excitation wavelength. Any increase in donor brightness in the second image compared with the first image is proportional to the energy that was previously transferred to the acceptor, or FRET (bottom right). If the molecules were not colocalizing, there will be no change in donor emission intensity, and no FRET (bottom left). (B) GSD-FRET analysis of colocalization between anti-γH2AX (donor) and anti-CUX1 (acceptor) in K562 cells. Scale bar, 1 μm. Bottom row images are following depletion of the acceptor fluorophore. Scale bar, 0.25 μm. Inset, representative FRET. Scale bar, 0.25 μm. Images shown are representative of results from 3 independent experiments. (C) Representative immunoblot for CUX1 protein in gHPRT and gCUX1 K562 cells (n = 3). (D) Principal component analysis of the histone posttranslational matrix (PTM) generated with EpiProfile analysis of histone PTMs in irradiated and mock-irradiated gHPRT and gCUX1 K562 cells. Histones were extracted 1 hour following irradiation (6 Gy). Results shown are derived from analysis of 3 independent samples. (E) Immunofluorescence imaging for EHMT2 and γH2AX colocalization 1 hour after irradiation (6 Gy). Colocalization was quantified in gHPRT and gCUX1 K562 cells after irradiation with or without the addition of an EHMT2 inhibitor, UNC0642, 60 minutes prior to irradiation. The fraction of colocalized pixels was calculated per nucleus. Results shown are a composite of 4 independent experiments. Significance was determined with a Student *t* test between indicated samples. (F) EpiProfile analysis of H3K27 methylation in irradiated and mock-irradiated gHPRT and gCUX1 K562 cells. Histones were extracted 1 hour following irradiation (6 Gy). Significance was determined with a Student *t* test between indicated samples. Results shown are derived from analysis of 3 independent samples. (G) ChIP-seq of H3K27me3 in K562 cells. Volcano plot showing differentially occupied ChIP-seq sites (n = 2) between clonal gHPRT and gCUX1 K562 cell lines. Each point is the average of 2 replicates. DiffBind was used to identify significantly differentially occupied sites. Red points indicate significance ≤10% FDR. (H) The panels depict a smooth line fit to the average column-wise read density for all differentially bound sites across the 20-kb window. Top panel, all H3K27me3 sites; bottom, only H3K27me3 sites significantly decreased in gCUX1 cells (10% FDR) (binomial *P* value = 7.35×10^{-60}). (I) The normalized read density is quantified at all H3K27me3 sites and at H3K27me3 sites lost in gCUX1 cells. A Mann-Whitney test was used to determine significance. IR, irradiation RPKM, reads per kilobase mapped reads.

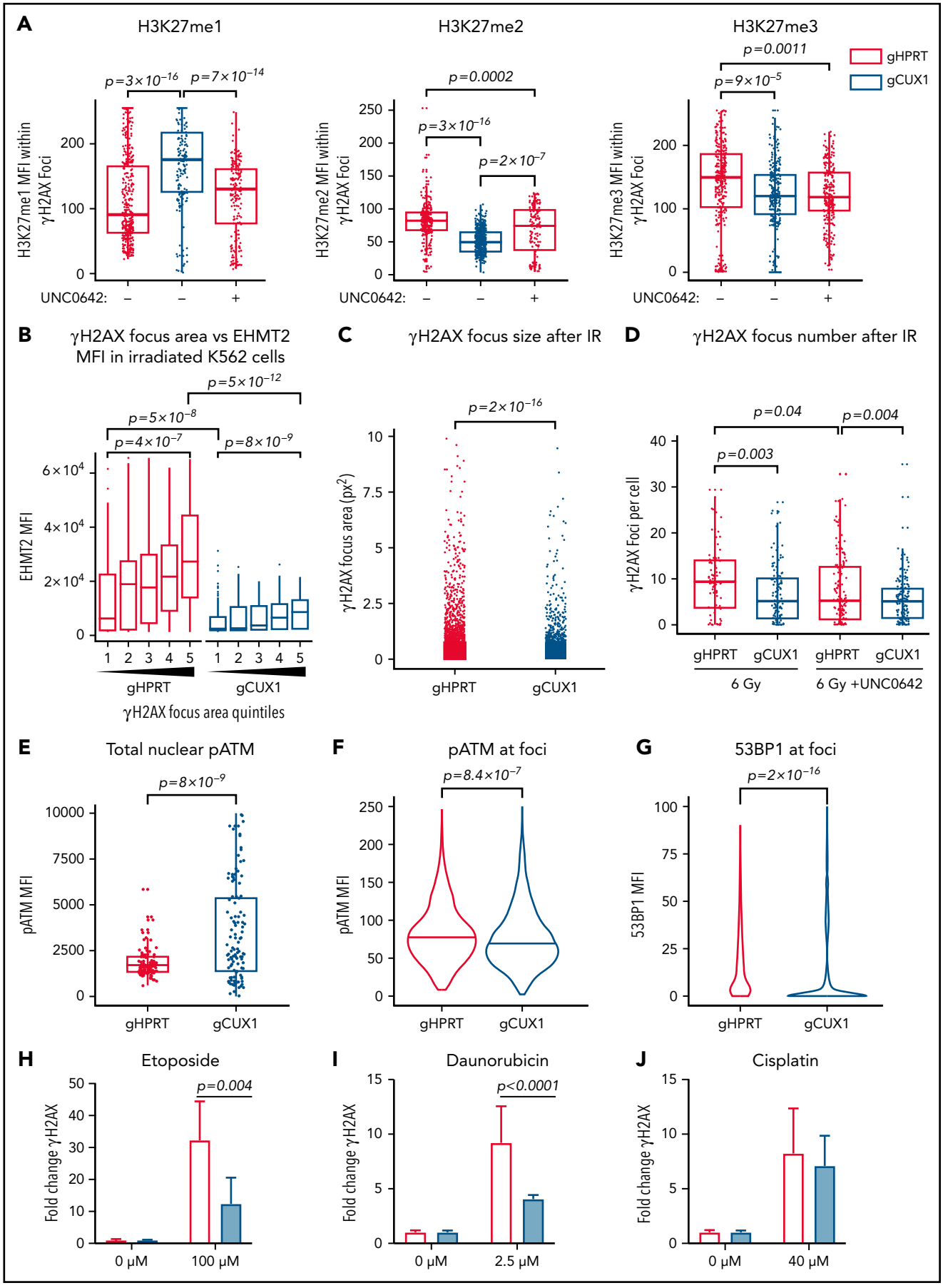

Figure 2.

knockdown of *CUX1*[20,35] (supplemental Figure 1B). We then explored other known functions of CUX1 that could impact the local DDR. CUX1 has been reported to regulate *CDKN1A* transcription via the recruitment of the histone methyltransferase EHMT2 (G9a).[36] In addition to regulating transcription,[36-38] EHMT2 promotes DSB repair by stabilizing activated ATM, necessary for downstream repair factor recruitment.[39,40] We therefore hypothesized that CUX1 regulates DNA repair at the epigenetic level via EHMT2. To initially test this model, we used clustered regularly interspaced short palindromic repeats (CRISPR)/CRISPR-associated protein 9 (Cas9) to target *CUX1* (gCUX1) or *HPRT* (gHPRT) as a control in K562 cells (Figure 1C). We assayed global histone posttranslational modifications 1 hour following irradiation in these cells using mass spectrometry.[41] Known histone modifications induced by irradiation, including dimethylation of H3K36 (fold-change 1.8; $q = 0.13$)[42] and acetylation of H3K18 (fold-change = 4.1; $q = 0.001$),[43] were appropriately increased in gHPRT cells following irradiation (supplemental Table 1), indicating that we detected relevant irradiation-induced modifications. Principal component analysis of the histone posttranslational modification matrix showed that although irradiation induced changes in histone modifications in gHPRT cells (principal component 1, 31.8% of variance), these changes did not occur in gCUX1 cells, and irradiated and unirradiated gCUX1 samples clustered together, separately from gHPRT cells (principal component 2, 16.8% of variance) (Figure 1D). These results indicate that: (1) CUX1-deficient cells have aberrant epigenetic marks at the basal state and (2) CUX1 is necessary for DNA damage–induced histone alterations following irradiation.

To test whether CUX1 recruits EHMT2 to sites of DNA damage, we imaged irradiated gHPRT and gCUX1 cells. Although EHMT2 colocalized with γH2AX in gHPRT control cells (as previously reported[44]), this colocalization was significantly reduced in gCUX1 cells (Figure 1E). As an additional control, we treated cells with the EHMT2 inhibitor, UNC0642.[45] The addition of UNC0642 to gHPRT cells reduced EHMT2-γH2AX colocalization to the extent seen in gCUX1 cells. The inhibitor did not, however, further decrease EHMT2-γH2AX colocalization in gCUX1 cells, suggesting that CUX1 acts upstream of EHMT2 recruitment (Figure 1E). We confirmed the role of CUX1 in EHMT2 localization to DSBs by GSD-FRET. In agreement with the immunofluorescence data, we found significantly decreased EHMT2-γH2AX interaction in gCUX1 cells, without changes in EHMT2 protein levels (supplemental Figure 1C-D). Overall, we find that CUX1 is required for the recruitment of EHMT2 to sites of DNA damage.

Best recognized for dimethylating H3K9, EHMT2 can also catalyze the mono- and dimethylation of H3K27.[46-48] EHMT2 also promotes H3K27 trimethylation through direct interaction with EZH2, a member of the polycomb repressive complex 2 (PRC2).[49] H3K27 and H3K9 methylation both play important roles in the early DDR.[40,44,50] To determine whether impaired EHMT2 recruitment in CUX1-deficient cells attenuates damage-induced histone methylation, we examined our proteomics data. H3K9me2 was among the 10 most upregulated marks following irradiation in gHPRT cells (fold-change, 9.23). H3K9me2 and H3K9me3 were decreased postirradiation in gCUX1 chromatin, although this did not achieve statistical significance ($P = .11$; $P = .13$; supplemental Figure 1E). H3K9me1 was increased after irradiation in both gHPRT and gCUX1 cells, with significantly more H3K9me1 in gCUX1 cells (supplemental Figure 1E). As methylation of H3K9 to form H3K9me2/3 is upregulated in DDR,[51] increased H3K9me1 could be due to a failure to convert H3K9me1 to H3K9me2/3 after irradiation in gCUX1 cells. On the other hand, H3K27me2 and H3K27me3 levels were significantly lower in gCUX1 cells compared with gHPRT cells, whereas H3K27me1 was upregulated appropriately after irradiation. Although the H3K27me2 phenotype was largely damage-dependent, H3K27me3 was significantly decreased both in irradiated and unirradiated gCUX1 cells (Figure 1F). In summary, global DNA damage–induced H3K9 and H3K27 methylation is disrupted by CUX1 loss, with more significant perturbation of H3K27 di- and trimethylation.

Given that H3K27me3 was decreased in both untreated and irradiated gCUX1 cells, we next determined the basal level of H3K27me3 by chromatin immunoprecipitation (ChIP) sequencing (ChIP-seq). Differential analysis revealed 848 loci with significantly decreased H3K27me3 in gCUX1 K562 cells compared with just 130 sites that gained H3K27me3 (10% false discovery rate [FDR]). H3K27me3 occupancy was also significantly decreased across all peaks (Figure 1G-I; supplemental Table 2). This global decrease in H3K27me3 in unirradiated gCUX1 cells corroborates our proteomics data and suggests that CUX1 loss impairs H3K27 methylation. The expression of H3K27 methyltransferases or demethylases was not altered by CUX1 knockdown in $CD34^+$ HSPCs or K562 cells (supplemental Figure 2A-B).[20,35,52] This finding implicates a nontranscriptional role for CUX1 in steady-state and DNA damage–induced H3K27me2/3 deposition.

CUX1 is necessary for DNA repair and focus formation

We next investigated whether the global decreases in H3K9 and H3K27 methylation seen after irradiation in CUX1-deficient cells were due to a loss of methylation specifically at sites of DNA damage. To investigate DSB-proximal histone methylation, we used immunofluorescence imaging to quantify methylation within γH2AX foci. Following irradiation, H3K9me1, H3K9me2, and H3K9me3 were significantly decreased at γH2AX foci in gCUX1 cells, although differences in total H3K9me1/2/3 were not detectable by western blot (supplemental Figure 2C-D). H3K27 monomethylation was increased, whereas H3K27 di- and trimethylation were significantly decreased at γH2AX foci after irradiation in gCUX1 K562 cells compared with gHPRT cells

Figure 2. CUX1 is necessary for DNA repair and focus formation. K562 cells were irradiated (6 Gy) and imaged 1 hour postirradiation. (A) Cells were imaged for antibodies targeting γH2AX and H3K27 methylation. H3K27me1/2/3 mean fluorescent intensity (MFI) was quantified within each γH2AX foci. (B) γH2AX foci size was quantified and broken into quintiles by size, with Q1 containing the smallest foci, and Q5 the largest. The size of individual γH2AX foci was determined using a custom ImageJ macro. EHMT2 intensity was quantified by MFI within each γH2AX foci quintile. (C) γH2AX foci size in gHPRT and gCUX1 cells (D) Mean number of γH2AX foci per cell following irradiation with and without UNC0642. (E) The intensity of total pATM (MFI) per nucleus was quantified after irradiation. (F) The intensity of pATM within γH2AX foci. (G) The intensity of 53BP1 within γH2AX foci. The median is shown, and a Mann-Whitney test was performed. (H-J) γH2AX was measured by flow cytometry in gHPRT and gCUX1 cells after 6 hours of mock treatment, etoposide (H), daunorubicin (I), or cisplatin (J). A Mann-Whitney test was performed. All plots are compiled from data derived from 3 independent biological replicates.

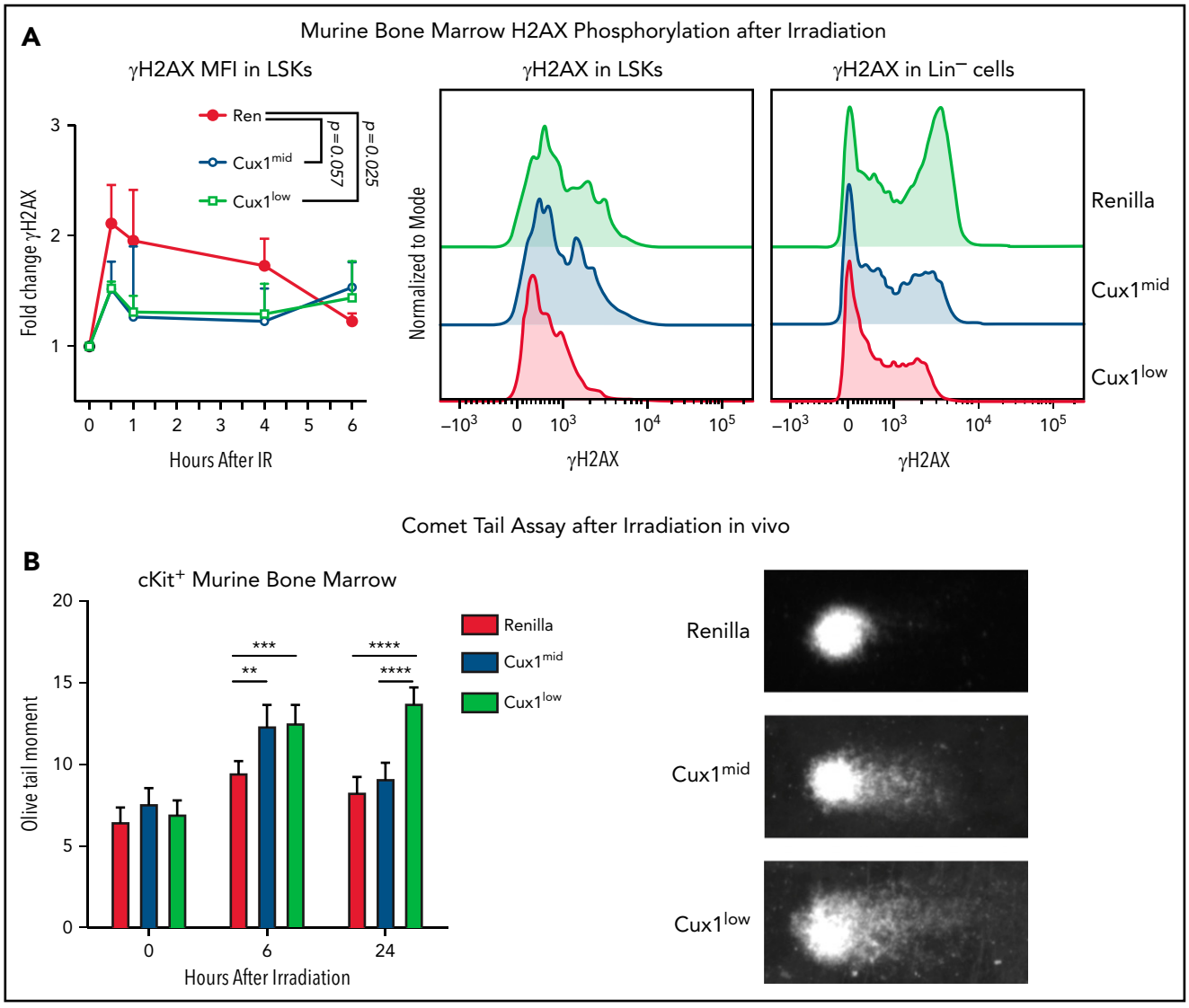

Figure 3. CUX1-deficient HSPCs have an impaired DNA damage response and unrepaired DNA damage in vivo. (A) Bone marrow (BM) was collected from Ren, Cux1^{mid}, and Cux1^{low} mice after treatment with Dox for 7 days. The cells were irradiated ex vivo (2 Gy) and γH2AX induction was measured by intracellular flow cytometry at 30 minutes, 1 hour, 4 hours, and 6 hours after irradiation. LSK cells were gated, and γH2AX MFI was normalized to the 0-hour timepoint from each experiment. Representative histograms of γH2AX staining 1 hour after irradiation in LSKs and total lineage-negative cells are shown. Plot is the result of 3 independent biological replicates. Data are shown as mean ± standard deviation (SD) with *P* values from a 2-way analysis of variance (ANOVA). (B) Ren, Cux1^{mid}, and Cux1^{low} mice were treated with Dox for 7 days and subsequently irradiated in vivo (6 Gy). Bone marrow was collected at 6 and 24 hours postirradiation, and Kit^{+} cells were isolated for a neutral comet assay. Representative images are shown (right). Mean ± standard error of the mean (SEM) is shown for 3 biological replicates. Mann-Whitney test, $^{*}P < .05$; $^{**}P < .01$; $^{***}P < .001$; $^{****}P < .0001$.

(Figure 2A). Inhibition of EHMT2 using UNC0642 in gHPRT cells recapitulated the loss of CUX1, with significantly decreased H3K27me2 and H3K27me3 within γH2AX foci (Figure 2A). Thus, CUX1 is necessary for H3K9me1/2/3 and H3K27me2/3 deposition at sites of DNA damage.

EHMT2 was reported to be required for sustained retention of activated, phosphorylated ATM (pATM) at DSBs for signal amplification and foci spreading.[39] To determine whether CUX1 is required for EHMT2-mediated focus formation or spreading, we quantified the relationship between EHMT2 accumulation and γH2AX foci size 1 hour after irradiation. In gHPRT cells, EHMT2 accumulation correlates with increasing foci size, suggesting that EHMT2 recruitment is permissive for foci spreading (Figure 2B). This correlation was maintained in gCUX1 cells, with increasing foci size corresponding to increased EHMT2, albeit with markedly decreased overall recruitment of EHMT2 (Figure 2B). This led us to hypothesize that γH2AX foci would be smaller and less numerous in gCUX1 cells. Indeed, 1 hour after irradiation, loss of CUX1 led to significantly smaller γH2AX foci (Figure 2C), and decreased foci numbers (Figure 2D). Similarly, treating gHPRT cells with UNC0642 led to decreased foci numbers, reducing γH2AX foci to the level seen in gCUX1 cells. UNC0642 treatment did not further reduce foci counts in gCUX1 cells (Figure 2D). These data indicate that CUX1 is necessary early in the repair process, upstream of H2AX phosphorylation and propagation.

To determine whether decreased γH2AX foci size in gCUX1 cells was due to a failure to retain pATM at breaks, we performed immunofluorescence imaging for pATM after irradiation. ATM

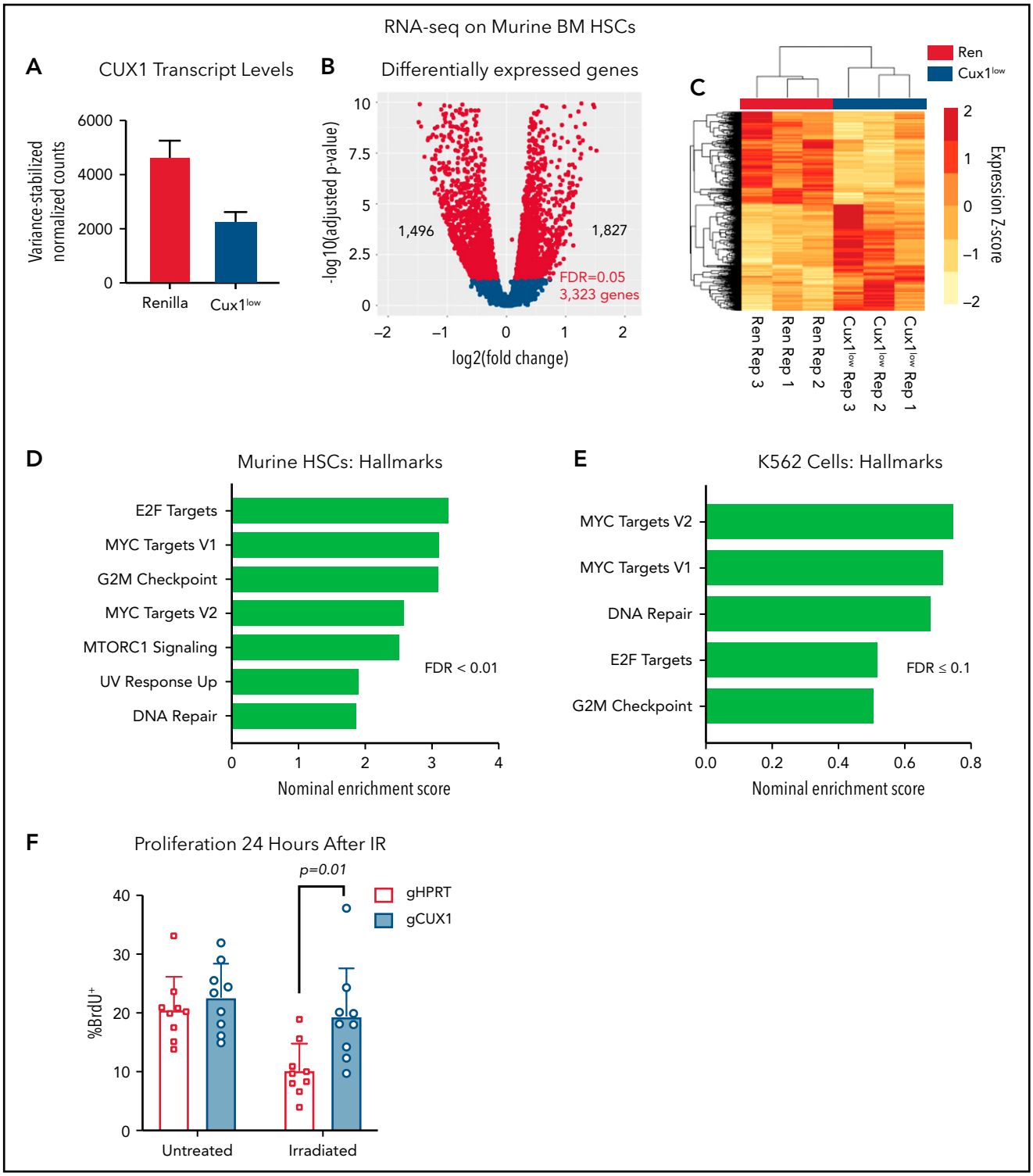

Figure 4. UX1-deficient cells upregulate expression of genes involved in proliferation and DNA repair. (A) Ren and Cux1^{low} mice were treated with Dox for 5 days, and HSCs (lineage-negative/cKit$^+$/Sca1$^+$/CD135$^-$) were sorted for RNA-seq, for a total of 3 biological replicates. *Cux1* transcript levels (excluding *Casp* isoforms) by RNA-seq are shown. (B) Volcano plot showing gene-expression changes in HSCs by RNA-seq after CUX1 knockdown. Blue color indicates differentially expressed genes with an FDR <5%. (C) A heatmap clustering the samples by the 3323 differentially expressed genes. The z score is indicated by the box color (scale on right). (D-E) Gene-set enrichment analysis (GSEA) using the "Hallmarks" gene set from the MSig Database[56] of murine HSCs (D) and shRen and shCUX1 K562 cells (E)(previously published RNA-seq).[35] Hallmark gene sets involved in proliferation and DNA damage repair with an FDR ≤0.1 are shown. Nominal enrichment score (NES) is plotted. (F) Twenty-four hours after irradiation (6 Gy) or mock irradiation, proliferation was assessed in gHPRT and gCUX1 K562 cells via BrdU incorporation 1 hour before analysis. Mean ± SD is shown for 3 biological replicates. Significance was determined with a Student *t* test between indicated samples.

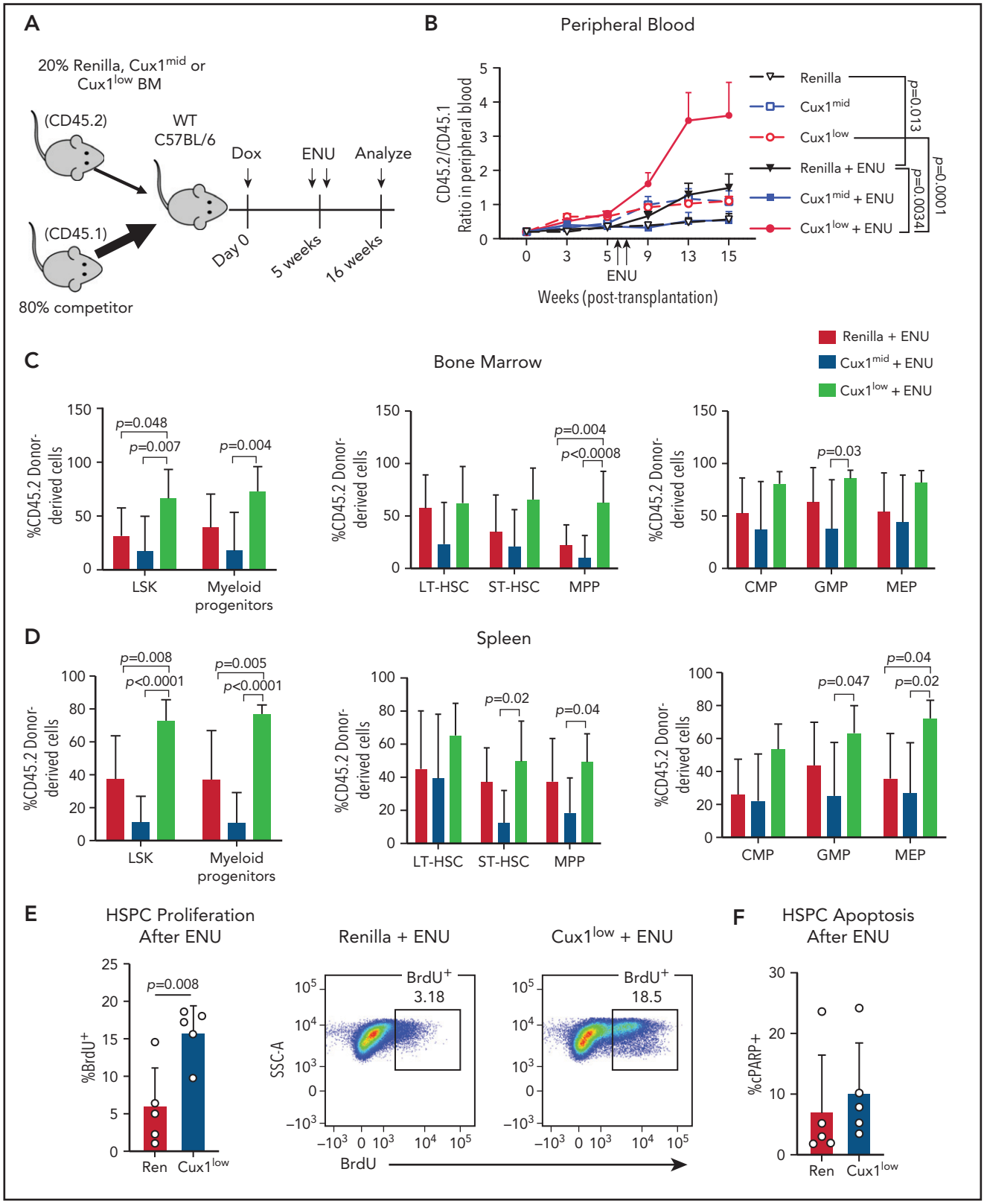

Figure 5. Cux1^{low} cells aberrantly proliferate and expand following DNA-damaging alkylating agents. (A) Bone marrow from Ren, Cux1^{mid}, and Cux1^{low} mice was transplanted at a 1:4 ratio with competitor bone marrow, and recipients were treated continuously with Dox beginning the day of transplant. Two doses of ENU (100 mg/kg) were administered 9 days apart, starting 5 weeks after transplant. (B) The contributions of Ren (n = 9), Cux1^{mid} (n = 8), and Cux1^{low} (n = 9) cells to the peripheral blood were monitored by flow cytometry. The ratio of Ren, Cux1^{mid}, or Cux1^{low} cells (CD45.2) to competitor cells (CD45.1) is shown. The mean ± SEM is shown. A mixed-effects analysis with the Geisser-Greenhouse correction is shown. Two independent biological replicates were performed (n = 4-5 mice per replicate per genotype). (C-D) At 16 weeks, the mice were euthanized and the contributions of Ren, Cux1^{mid}, and Cux1^{low} (CD45.2) to the hematopoietic stem and progenitor populations were measured by flow cytometry in the bone marrow (C) and spleen (D). LSK cells and myeloid progenitors (Lin$^-$/Sca1$^-$/c-Kit$^+$) are shown (left). LSK cells were further gated for long-term HSCs (LT-HSC; CD150$^+$/CD48$^-$), short-term HSCs (ST-HSC; CD48$^-$/CD150$^-$), and multipotent progenitors (MPP; CD48$^+$/CD150$^-$) (center). Within the progenitor

activation did occur in gCUX1 cells, with total nuclear pATM mean fluorescent intensity (MFI) elevated compared with gHPRT cells (Figure 2E). However, pATM was not retained at foci. pATM intensity within γH2AX foci was reduced in gCUX1 cells compared with gHPRT cells after irradiation (Figure 2F). As pATM retention at breaks is necessary for γH2AX foci spreading and downstream activation of DDR factors,[53] we next examined repair factor recruitment. Both H3K27me2/3[50] and EHMT2[40] have been independently reported to be required for efficient recruitment of 53BP1. We therefore performed imaging for 53BP1 and found decreased 53BP1 intensity at γH2AX foci in irradiated gCUX1 cells (Figure 2G). We investigated whether these findings extended to chemotherapy-induced DNA damage using 3 classes of chemotherapies linked to t-MNs: etoposide, a topoisomerase II inhibitor; daunorubicin, an anthracycline; and cisplatin, a platinum-based cross-linking agent.[1,54] We found significantly diminished γH2AX in gCUX1 cells compared with gHPRT cells following daunorubicin and etoposide treatments (Figure 2H-I). Following cisplatin treatment, γH2AX was slightly, but not significantly, decreased in gCUX1 cells compared with gHPRT (Figure 2J). In summary, CUX1-deficient cells fail to recruit EHMT2 to breaks and deposit H3K27me2/3, leading to decreased γH2AX focus formation and spreading, decreased local pATM, and decreased 53BP1 recruitment at sites of DNA damage.

CUX1-deficient HSPCs have an impaired DDR and unrepaired DNA damage in vivo

To determine whether the DNA repair defects in CUX1-deficient K562 cells in vitro are also present in primary CUX1-deficient hematopoietic cells in vivo, we used our Dox-inducible shRNA transgenic mouse models.[20] Cux1^{mid} and Cux1^{low} lines express distinct shRNAs targeting *Cux1* and have 58% and 42% residual *Cux1* messenger RNA expression , respectively, in hematopoietic lineage-negative/Sca-1^{+}/Kit^{+} cells (LSKs).[20] Littermates expressing an shRNA targeting Ren were used as controls (Ren). We first assessed whether CUX1-deficient HSPCs exhibit reduced γH2AX focus formation. In agreement with our human cell line data, we found that CUX1-deficient HSPCs showed attenuated phosphorylation of H2AX following irradiation. This was true in both LSKs and lineage-negative cells (Figure 3A). After 6 hours, Ren γH2AX foci levels returned to baseline and were not significantly different from Cux1^{mid} and Cux1^{low}.

To assess whether CUX1 is required for break repair, in addition to break recognition, we performed neutral comet assays to measure DSBs in HSPCs.[55] Following a single dose of whole-body irradiation, Cux1^{mid} and Cux1^{low} HSPCs show significantly elevated levels of DSBs 6 hours postirradiation (Figure 3B). The unrepaired breaks persisted 24 hours after irradiation in Cux1^{low} HSPCs (Figure 3B). Thus, CUX1 deficiency leads to unrepaired DNA damage in HSPCs in vivo following irradiation. We find that, in both a human hematopoietic cell line and primary mouse HSPCs, CUX1 is required for recognition and resolution of DNA damage.

CUX1-deficient cells upregulate genes involved in proliferation and DNA repair

To further assess a potential transcriptional mechanism for disrupted γH2AX focus formation, we performed RNA-seq of Ren and Cux1^{low} HSCs (Lin^{-}/Kit^{+}/Sca1^{+}/CD135^{-}) after 5 days of Dox (supplemental Table 3). By RNA-seq, *Cux1* transcripts were ~50% decreased in Cux1^{low} HSCs (Figure 4A). We identified 3323 differentially expressed genes (FDR, <5%): 1827 genes were upregulated after CUX1 knockdown and 1496 genes were downregulated (Figure 4B-C). As in human CD34^{+} HSPCs and K562 cells, CUX1 knockdown did not lead to decreased gene expression of H3K27 methyltransferases or increased transcription of demethylases (supplemental Figure 3A). Gene-set enrichment analysis[56] showed that *Cux1* knockdown drives proliferative signatures, including genes activated by E2F and MYC and genes involved in G_2/M checkpoint progression (Figure 4D). We did not find genes regulating the DDR decreased (fold-change less than −0.5) after *Cux1* knockdown and, in fact, we found an upregulation of "DNA Repair" and "UV Response Up" gene sets, possibly reflecting a compensatory mechanism for unresolved damage. In agreement with CD34^{+} HSPCs and K562 data, transcription of *Atm* and *Atr* were unchanged (supplemental Figure 3B). RNA-seq data from shCUX1 K562 cells also showed upregulation of proliferation and DNA repair pathways (Figure 4E).[35] The results from RNA-seq of Ren and Cux1^{low} HSPCs, demonstrating enrichment of proliferative signatures at baseline, are consistent with the previously reported RNA-seq in human CD34^{+} HSPCs, and the hypercellular bone marrow and decreased quiescence detected in Cux1^{low} mice at baseline.[20] Thus, CUX1 knockdown in primary murine HSCs leads to upregulation of proliferation and DDR pathways.

Based on the impaired DDR in both CUX1-deficient K562 cells (Figure 2C-D) and murine HSPCs (Figure 3A), we predicted that CUX1-deficient cells proliferate despite unrepaired damage. To test this, we irradiated gHPRT and gCUX1 K562 cells and measured 5-bromo-2′-deoxyuridine (BrdU) incorporation 24 hours later. gHPRT cells exhibited reduced proliferation following irradiation-induced DNA damage, whereas gCUX1 cells did not (Figure 4F). There was not a significant difference in apoptosis between irradiated gHPRT and gCUX1 cells (supplemental Figure 3C). In summary, we find that CUX1-deficient cells continue to proliferate in the presence of DNA damage.

Cux1^{low} cells proliferate and expand following DNA-damaging alkylating agents

In patients, certain mutations provide HSPCs a fitness advantage in the context of chemotherapy, enabling those clones to expand.[11,57] We hypothesized that CUX1 deficiency would similarly provide a selective advantage under the pressure of chemotherapy. As alkylating agents are the most common chemotherapy exposure preceding t-MNs,[4] we used ENU, an alkylating agent well-characterized in mouse models to

Figure 5 (continued) population, cells were separated into common myeloid progenitors (CMP; CD34^{+}/CD16/32^{low}), granulocyte-monocyte progenitor (GMP; CD34^{+}/CD16/32^{high}), and megakaryocyte-erythroid progenitors (MEP; CD34^{-}/CD16/32^{-}) (right). The mean ± SD and *P* values from a 1-way ANOVA comparison are shown. Two independent biological replicates were performed. (E) Proliferation was measured in Ren and Cux1^{low} mice after ENU administration. Mice were given 2 doses of ENU, 9 days apart. Six hours after the second dose of ENU, BrdU was administered. BrdU^{+} cells were measured by flow cytometry 12 hours after BrdU injection in the bone marrow HPSC population (Lin^{-}). Representative flow plots are shown. The mean ± SD and Student *t* test *P* value is shown. (F) Apoptosis was measured in the same cells by flow cytometry using antibodies for cleaved poly (ADP-ribose) polymerase (cPARP). Three independent biological replicates were performed. SSC-A, side scatter area; WT, wild type.

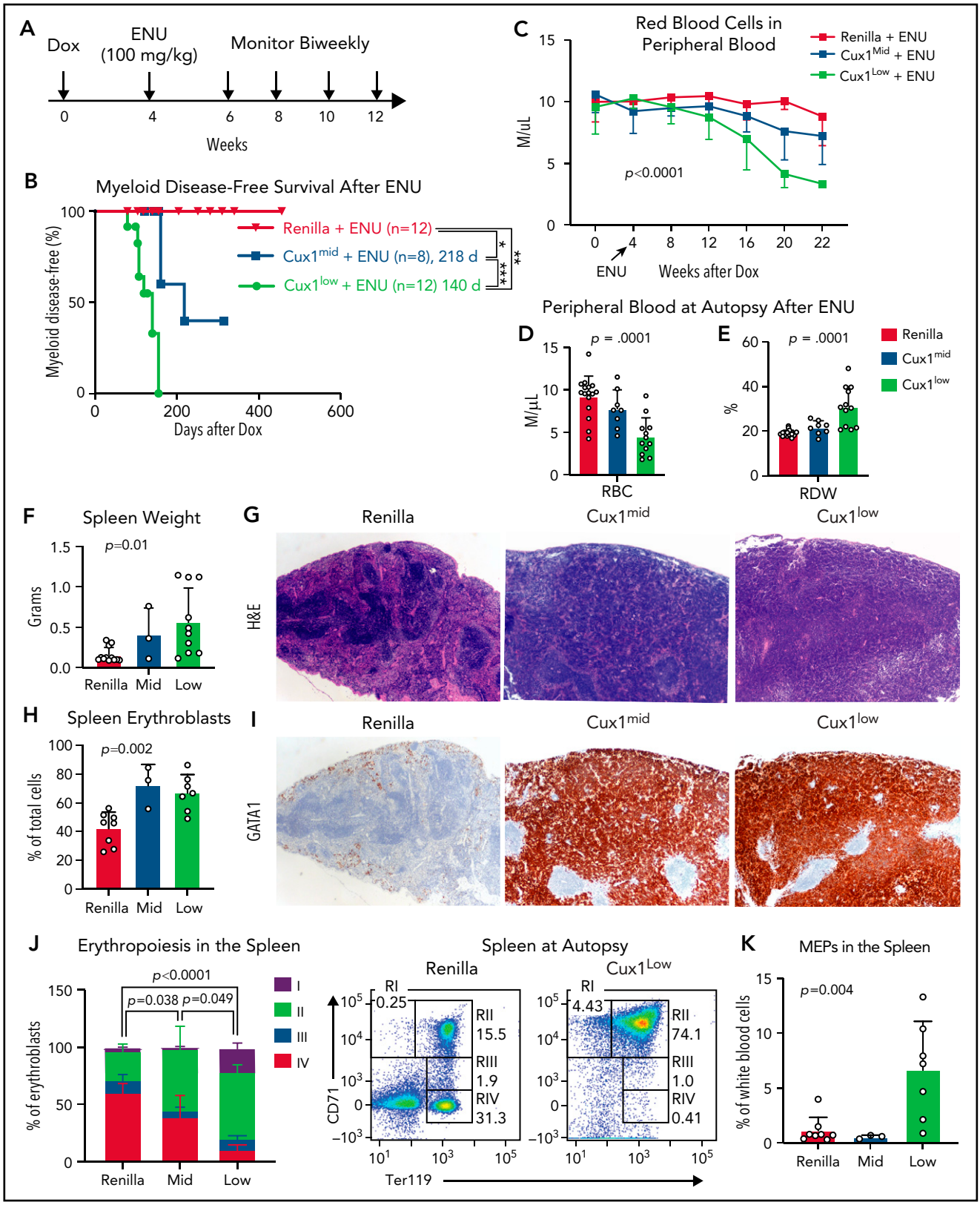

Figure 6. CUX1-deficient mice develop t-MNs after alkylator chemotherapy exposure. (A) Cux1^{mid}, Cux1^{low}, and littermate Ren mice were treated continuously with Dox to induce CUX1 knockdown. At 1 month, mice were treated with an alkylating agent, ENU (100 mg/kg). Peripheral blood was monitored on a biweekly basis. (B) Kaplan-Meier plot showing significantly increased myeloid disease incidence for Cux1^{mid} (n = 8) and Cux1^{low} (n = 12) mice treated with ENU compared with Ren mice treated with ENU (n = 12). Results are shown from 2 independent experiments (n = 4-6 mice per replicate). $^{**}P < .01$, $^{***}P < .001$, log-rank test . Median survival is shown. (C) Complete blood count analysis showing decreased RBC counts following ENU treatment in Cux1^{mid} and Cux1^{low} mice compared with Ren. The mean plus or minus SD is shown. A mixed-effects analysis with the Geisser-Greenhouse correction was performed. (D-E) Red blood cell count (RBC) (D) and red cell distribution width (RDW) (E) from complete

recapitulate chemotherapy in vivo.[58-61] We performed mixed bone marrow chimera experiments, with Ren, Cux1^{mid}, or Cux1^{low} donor bone marrow (CD45.2^{+}) and wild-type competitor bone marrow (CD45.1^{+}) (Figure 5A). Upon addition of ENU, Cux1^{low} cells exhibited a significantly increased contribution to the peripheral blood compared with either untreated Cux1^{low} or ENU-treated Ren cells (Figure 5B). At autopsy, ENU-treated Cux1^{low} cells constituted a significantly higher percentage of the LSKs and myeloid progenitors in the bone marrow and spleen (Figure 5C-D). Unlike Cux1^{low}, Cux1^{mid} cells did not expand after ENU in these experiments, which is consistent with the generally milder phenotypes observed in Cux1^{mid} mice that increase with age.[20] In summary, Cux1^{low} HSPCs have a competitive advantage following ENU.

We tested whether the blunted DDR in Cux1^{low} cells (Figure 3A) leads to a failure to halt proliferation post-DNA damage, as seen in gCUX1 K562 cells (Figure 4F). Cux1^{low} HSPCs showed increased BrdU incorporation in the 24 hours following ENU compared with controls, whereas untreated cells did not show a significant difference (Figure 5E; supplemental Figure 3D). There was no change in apoptosis (Figure 5F). Thus, we conclude that CUX1 deficiency drives a fitness advantage under the selective pressure of chemotherapy, characterized by persistent proliferation following DNA-damaging agents.

CUX1-deficient mice develop t-MNs after alkylator chemotherapy exposure

Recent studies suggest that, in many patients, preexisting mutant HSPCs expand and transform to t-MNs after chemotherapy.[6,57,62] Therapy-induced CHIP is enriched for DDR genes.[11,57] Thus, we investigated the link between defective DDR in CUX1-deficient cells and t-MN susceptibility. We treated Ren, Cux1^{mid}, and Cux1^{low} mice with Dox for 1 month, followed by chemotherapy (ENU, 100 mg/kg) (Figure 6A). A small number (n = 2 of 12; 17%) of the ENU-treated control mice developed lymphoid disease, consistent with a prior report,[59] but the majority of Ren mice had a normal lifespan. In the absence of chemotherapy, Cux1^{mid} mice spontaneously develop MDS but do not have decreased survival.[20] In contrast, ENU-exposed Cux1^{mid} mice have a significantly shortened lifespan (median survival, 160 days). Untreated Cux1^{low} mice succumb to MDS/MPNs (275 days).[20] Upon exposure to ENU, Cux1^{low} survival time is reduced by more than one-half (median survival, 124 days) (supplemental Figure 4A). We used the Bethesda criteria to identify myeloid disease after alkylator chemotherapy.[63] None of the Ren mice treated with ENU developed a t-MN, consistent with prior work.[59] In stark contrast, 38% (3 of 8; $P = .049$) of Cux1^{mid} and 83% (10 of 12; $P < .0001$) of Cux1^{low} mice developed myeloid disease, whereas the remaining presented with lymphoid disease (Figure 6B; supplemental Figure 4B). Of note, Cux1^{low} mice had accelerated onset ($P = .002$) and increased penetrance ($P = .035$) of t-MNs compared with Cux1^{mid}. These results demonstrate that CUX1 deficiency sensitizes mice to t-MNs in a dosage-dependent manner.

At the time of euthanasia for disease, most Cux1^{mid} and Cux1^{low} mice did not show changes in total peripheral blood white blood cell counts. However, myeloid skewing was evident by increased frequency of peripheral blood granulocytes and platelets in Cux1^{low} mice, with similar trends in Cux1^{mid} (supplemental Figure 4C-D). B cells (B220^{+}) were significantly decreased, and T cells (CD3e^{-}) were largely unchanged (supplemental Figure 4D). In Cux1^{low} mice, myeloid cells were expanded in the spleen and bone marrow, with Cux1^{mid} mice trending in the same direction (supplemental Figure 4E-F). Thus, post-ENU, Cux1^{mid}, and Cux1^{low} mice display myeloid hyperplasia.

In distinction to the MDS and MDS/MPN observed in CUX1-deficient mice,[20] ENU-treated CUX1-deficient mice develop acute erythroleukemia. Following ENU, RBC counts declined in Cux1^{mid} and Cux1^{low} mice (Figure 6C-D). This anemia was accompanied by an elevated RBC distribution width (RDW) (Figure 6E). Both Cux1^{mid} and Cux1^{low} mice display splenomegaly with a total effacement of splenic architecture (Figure 6F-G). The splenomegaly in Cux1^{mid} and Cux1^{low} mice was primarily driven by a marked expansion of erythroid precursors in the spleen, illustrated by intense and pervasive GATA1 immunohistochemical staining (Figure 6H-I). Normally, GATA1 predominates in scattered early erythroid forms, as seen in Ren spleens (Figure 6I). In erythroleukemia, GATA1 staining is uniformly intense, whereas other AML subtypes remain negative.[64] CUX1 knockdown led to decreased mature erythroblasts (RIV, orthochromatophilic, CD71^{-}/Ter119^{+}) in the spleen and bone marrow. The expanded erythroblast population in the spleen was mainly composed of immature RI (proerythroblasts, CD71^{+}/Ter119^{mid}) and RII (basophilic, CD71^{+}/Ter119^{+}) populations. The RI population was also increased in the bone marrow (Figure 6J; supplemental Figure 4G). We observed infiltration of these immature erythroid populations in nonhematopoietic tissues, including the liver, with varying penetrance (supplemental Figure 5A-B). Cux1^{low} mice, but not Cux1^{mid} mice, had significant expansion of megakaryocyte-erythroid progenitors (MEPs; Lin^{-}/CD34^{-}/FcγR^{low}/Kit^{+}/Sca-1^{-}) in the spleen (Figure 6K). The anemia, dramatic expansion of immature erythroid precursors, infiltration into the liver, and rapid onset of disease led us to characterize the disease in both Cux1^{mid} and Cux1^{low} mice as a therapy-related erythroleukemia.[63] Of note, erythroleukemia in patients is often associated with prior chemotherapy as well as −7/del(7q).[65,66] In summary, we find CUX1 deficiency predisposes mice to an aggressive t-MN, specifically an erythroleukemia.

Restoration of CUX1 prevents the development of a t-MN

The evidence that CUX1 regulates the DDR led us to investigate whether CUX1 loss leads to additional mutations that drive trans-

Figure 6 (continued) blood count analysis at autopsy. (F) The spleen weight at autopsy is shown for Ren, Cux1^{mid}, and Cux1^{low} mice. (G) Representative images from Ren, Cux1^{mid}, and Cux1^{low} spleens stained with hematoxylin and eosin (H&E) are shown; original magnification, ×40. (H) Erythroblasts (CD71^{+} or Ter119^{+}) in the spleen quantified as a percentage of total cells. (I) Representative Ren, Cux1^{mid}, and Cux1^{low} spleens stained for an immature erythroid marker, anti-GATA1. Original magnification, ×40. The mean ± SD and 1-way ANOVA *P* values are shown. (J) RI-RIV erythroid precursor populations quantified as a percentage of erythroblasts in the spleen. The mean ± SD is shown, and *P* values were calculated using a 2-way ANOVA. Representative flow plots for the erythroblast markers CD71 and Ter119 are shown. (K) MEPs in the spleen, as a percentage of white blood cells. The mean ± SD and 1-way ANOVA *P* values are shown. Panels F-K represent mice that develop nonlymphoid disease after ENU for Cux1^{mid} (n = 3) and Cux1^{low} mice (n = 10). *$P < .05$; **$P < .01$; ***$P < .001$; ****$P < .0001$.

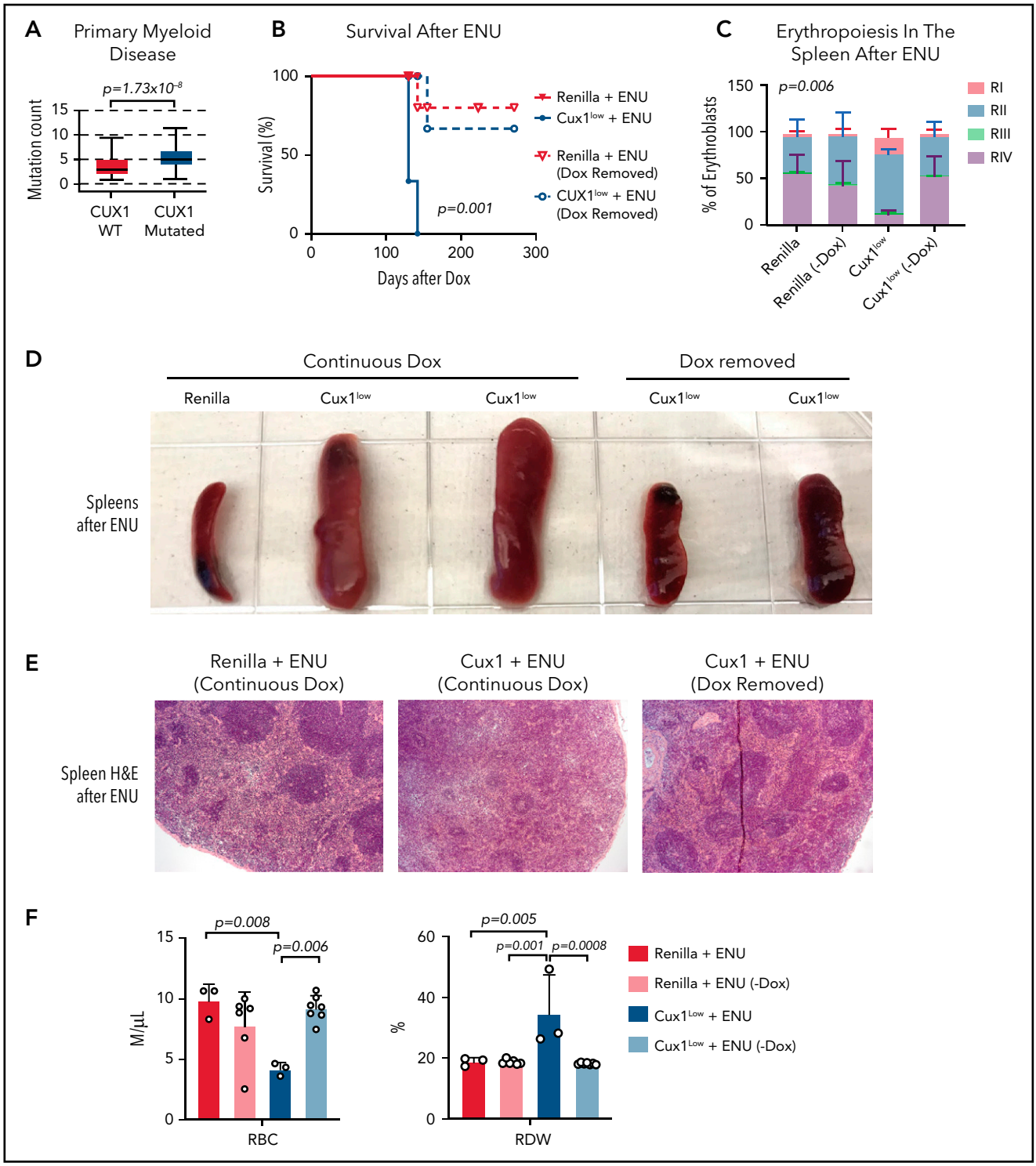

Figure 7. Sustained CUX1 loss is required for the development of t-MNs. Restoration of CUX1 prevents t-MNs. (A) Mutational burden in primary samples from patients with *CUX1*-wild type (n = 1731) and *CUX1* mutations or deep deletions (n = 35). Samples are from patients with myeloid neoplasms, including AML, MDS, MPN, and MDS/MPN. AACR GENIE Cohort v9.0[88] (B) Ren and Cux1^{low} mice were treated with Dox and ENU as in Figure 6. One month after ENU, Dox was removed and CUX1 expression restored in a cohort of Ren (n = 6) and Cux1^{low} (n = 7) mice (dashed lines). A cohort of Ren (n = 3) and Cux1^{low} (n = 3) mice continued to receive Dox (solid lines). Ren mice were euthanized when Cux1^{low} mice showed signs of disease. (C) RI-RIV erythroid precursor populations quantified as a percentage of erythroblasts in the spleen. The mean ± SD is shown, and *P* values were calculated using a 2-way ANOVA. (D) Representative images of spleens at autopsy from Ren and Cux1^{low} mice at autopsy. (E) Representative images from Ren and Cux1^{low} spleens stained with H&E are shown; original magnification, ×40. (F) RBC count and RDW from complete blood count analysis at autopsy. The mean ± SD and 1-way ANOVA comparison *P* values are shown.

formation. We found that, in primary patient samples, *CUX1* mutations were associated with a higher mutational burden in myeloid neoplasms (Figure 7A). We next asked whether these mutations were driving transformation, or whether CUX1 had additional tumor-suppressive roles. If the former, we reasoned that CUX1 deficiency at the time of DNA damage should be sufficient to

acquire mutations and transform. To test this, we administered ENU to Dox-treated Ren and Cux1^{low} mice, then restored *Cux1* expression 30 days later via Dox withdrawal. Restoring *Cux1* prevented myeloid transformation, rescued erythroid differentiation, and prevented splenomegaly and anemia (Figure 7B-F). Thus, although the impaired DDR allows for proliferation despite damage (Figures 4F and 5E), sustained CUX1 knockdown is required for the development of a t-MN. This is consistent with the known roles for CUX1 in hematopoietic differentiation and proliferation.[20,21]

Discussion

t-MN remains an inherently treatment-resistant cancer. Although identifying novel drug targets is of paramount importance, equal, if not greater, emphasis should be placed on prevention. The field is now equipped with emerging biomarkers, including germline risk alleles and somatic CHIP mutations. Determining how these genetic changes interact with environmental exposures is the missing link in understanding and preventing the evolution of t-MNs. Here, we show that preexisting CUX1-deficient HSPCs cells fail to recognize and repair DNA damage, expand, and transform to a t-MN. Based on this, we speculate that *CUX1* mutations and −7/del(7q) are biomarkers for t-MN risk.

EHMT2 plays a key role in the DDR through methylation of histones and MDC1 to promote pATM stabilization and downstream repair factor recruitment.[39,40,67] Nevertheless, the factor responsible for recruiting EHMT2 to DSBs was unknown.[39,49] Here, we report a novel function for CUX1 in this role. CUX1 deficiency phenocopies loss of EHMT2 in several regards, including decreased pATM stabilization at foci without impaired ATM activation.[39] In agreement with the reports of roles for EHMT2 and H3K27me3 in nonhomologous end joining,[40,50] we observe that CUX1 loss impairs histone methylation and 53BP1 recruitment. Intriguingly, it has been reported that reduced H3K27me2/3 at sites of DNA damage leads to reduced 53BP1 binding and nonhomologous end joining, but increased binding of FANCD2.[50] These findings position CUX1 as an early player in the DDR, possibly involved in repair pathway choice.

Another possibility is that *CUX1* and *EZH2* mutations cooperate to drive t-MN. Of 7q genes, only *CUX1*, *EZH2*, and *LUC7L2* mutations are associated with shorter survival, and, interestingly, these mutations are not mutually exclusive.[68] Unlike *Cux1*, *Ezh2* loss alone does not lead to myeloid neoplasms in mice.[69] These mutations may synergize, similar to the effect of −7 or long deletions of 7q.

A common theme manifesting in t-MNs is the importance of intact DNA repair machinery. Twenty-one percent of t-MN patients harbor inherited mutations in DDR genes.[70] CHIP mutations in DDR genes are particularly associated with t-MN.[11,57,70-73] *TP53* is a well-described example of this paradigm, in the contexts of both inherited and CHIP mutations.[61,74] However, *TP53* inactivation accounts for <30% of t-MN patients.[70,75] Furthermore, defective DDR may not be sufficient to cause t-MNs. For instance, Tp53$^{+/-}$ mice do not have increased incidence of alkylator-induced myeloid disease.[76-78] Mutations acquired through ineffective DNA repair also do not seem to be a driving force in tumorigenesis, as tumor-suppressor genes with known roles in DNA damage, such as *TP53*, are not associated with a higher mutational burden.[79] This is supported by our data showing that, although *CUX1* mutations are associated with a higher mutational burden, sustained CUX1 deficiency is still required for transformation to a t-MN. Although this increased mutational burden is consistent with a prior report on a small number of patients,[26] future studies substantiating this increased mutational burden in larger, more uniform populations of patients are warranted. By nature of its role in multiple facets of tumorigenesis, that is, differentiation, proliferation, and DNA repair, CUX1 may be a particularly potent tumor suppressor and driver of t-MNs. This is supported by the protective effect of restoring CUX1 in t-MN development, presenting a possible therapeutic avenue.

It is noteworthy that the HSC DDR declines with age,[80-83] as do *CUX1* levels.[84,85] The combination may be particularly oncogenic; that is, with age, *CUX1* levels drop past a critical threshold that is eventually permissive for clonal expansion and transformation. This may explain the reduced clonal expansion by Cux1^{mid} HSPCs following therapy (Figure 5). The Cux1^{mid} mice model, a milder knockdown of CUX1 and, indeed, myeloid transformation, is only seen after aging[20] or therapy (Figure 6). This may partly explain why −7/del(7q) myeloid malignancies increase with age.[1,4,86] By identifying a critical gene associated with clonal selection and transformation, our work paves the way for identifying patients at risk for t-MNs.

Acknowledgments

The authors thank Michelle Le Beau, Angela Stoddart, Madhavi Senagolage, and Stephen Arnovitz for critical reading of the manuscript. The authors are grateful for the services and assistance provided by the following University of Chicago core facilities supported by the Cancer Center Support Grant (P30 CA014599): Christine Labno and The University of Chicago's Integrated Light Microscopy Core Facility, Pieter Faber and the High Throughput Genomics Core Facility (RRID: SCR_019196), David Leclerc in the Flow Cytometry Facility (RRID: SCR_017760), and the Human Tissue Resource Center (RRID:SCR_019199). The authors also thank Chuanhong Liao in the Biostatistics Laboratory for special assistance and services, as well as The University of Chicago Center for Research Informatics and Animal Resources Center. The authors thank Michelle Le Beau and Le Beau laboratory members for sharing advice, reagents, and resources. The authors acknowledge the American Association for Cancer Research (AACR) and its financial and material support in the development of the AACR Project Genomics Evidence Neoplasia Information Exchange (GENIE) registry, as well as members of the consortium for their commitment to data sharing.

This work was supported, in part, by the American Cancer Society Research Scholar Grant (M.E.M.), the American Society of Hematology Junior Faculty Scholar Award (M.E.M.), the National Institutes of Health (National Heart, Lung, and Blood Institute grant HL142782 and National Cancer Institute grant CA231880 [M.E.M.]; National Cancer Institute grant R21CA213247 [S.J.K.]), the Brinson Foundation (M.E.M.), and Robin and Matthew Patinkin and The University of Chicago Cancer Research Foundation Women's Board (M.E.M.). M.K.I. was supported by National Institutes of Health, National Cancer Institute grant F30CA232673 and The University of Chicago Medical Scientist Training Program (National Institute of General Medical Sciences grant T32GM007281). J.L. was supported by Multidisciplinary Training Program in Cancer Research (MTCR) grant T32 CA009594 from the National Institutes of Health, National Cancer Institute. Interpretations are the responsibility of the study authors. The visual abstract was created with BioRender.com.

Authorship

Contribution: M.K.I. designed and performed experiments, interpreted data, and wrote the manuscript; J.L. performed experiments and edited the manuscript; N.A. performed experiments and provided conceptual and technical advice; B.H. performed experiments; S.K. performed western blots and CHIP-seq; J.K. performed the CHIP-seq analysis; T.C.M.

performed western blots; D.W. prepared the proteomics samples and did initial PTM analysis using EpiProfile; S.K.G. performed hematopathologic analyses and edited the manuscript; S.J.K. interpreted data and edited the manuscript; and M.E.M. conceived the experiments, interpreted data, and edited the manuscript.

Conflict-of-interest disclosure: S.J.K. received a research grant from AbbVie, receives royalties from Millipore, and has ownership of Cell IDx, OncoSenescence, Transnostics, and BioFluid Technologies. The remaining authors declare no competing financial interests.

ORCID profiles: M.K.I., 0000-0003-3724-5338; B.H., 0000-0001-8970-3201; T.C.M., 0000-0002-7074-9610; D.W., 0000-0002-8960-338X; S.K.G., 0000-0003-0716-8730; S.J.K., 0000-0003-1518-2436; M.E.M., 0000-0002-8260-3598.

Correspondence: Megan E. McNerney, Department of Pathology, University of Chicago, 5128 Knapp Center for Biomedical Discovery, 900 East 57th St, Chicago, IL 60637; e-mail: megan.mcnerney@uchospitals.edu.

Footnotes

Submitted 16 September 2020; accepted 23 April 2021; prepublished online on *Blood* First Edition 27 May 2021. DOI 10.1182/blood.2020009195.

The data reported in this article have been deposited in the Gene Expression Omnibus[87] database (accession number GSE154674).

The authors will respond to requests for data e-mailed to the corresponding author.

The online version of this article contains a data supplement.

There is a *Blood* Commentary on this article in this issue.

The publication costs of this article were defrayed in part by page charge payment. Therefore, and solely to indicate this fact, this article is hereby marked "advertisement" in accordance with 18 USC section 1734.

REFERENCES

1. Smith SM, Le Beau MM, Huo D, et al. Clinical-cytogenetic associations in 306 patients with therapy-related myelodysplasia and myeloid leukemia: the University of Chicago series. *Blood*. 2003;102(1):43-52.
2. Fianchi L, Pagano L, Piciocchi A, et al. Characteristics and outcome of therapy-related myeloid neoplasms: Report from the Italian network on secondary leukemias. *Am J Hematol*. 2015;90(5):E80-E85.
3. de Moor JS, Mariotto AB, Parry C, et al. Cancer survivors in the United States: prevalence across the survivorship trajectory and implications for care. *Cancer Epidemiol Biomarkers Prev*. 2013;22(4):561-570.
4. McNerney ME, Godley LA, Le Beau MM. Therapy-related myeloid neoplasms: when genetics and environment collide. *Nat Rev Cancer*. 2017;17(9):513-527.
5. Gibson CJ, Lindsley RC, Tchekmedyian V, et al. Clonal hematopoiesis associated with adverse outcomes after autologous stem-cell transplantation for lymphoma. *J Clin Oncol*. 2017;35(14):1598-1605.
6. Takahashi K, Wang F, Kantarjian H, et al. Preleukaemic clonal haemopoiesis and risk of therapy-related myeloid neoplasms: a case-control study. *Lancet Oncol*. 2017;18(1):100-111.
7. Young AL, Challen GA, Birmann BM, Druley TE. Clonal haematopoiesis harbouring AML-associated mutations is ubiquitous in healthy adults. *Nat Commun*. 2016;7:12484.
8. Bowman RL, Busque L, Levine RL. Clonal hematopoiesis and evolution to hematopoietic malignancies. *Cell Stem Cell*. 2018;22(2):157-170.
9. Jaiswal S, Fontanillas P, Flannick J, et al. Age-related clonal hematopoiesis associated with adverse outcomes. *N Engl J Med*. 2014;371(26):2488-2498.
10. Genovese G, Kähler AK, Handsaker RE, et al. Clonal hematopoiesis and blood-cancer risk inferred from blood DNA sequence. *N Engl J Med*. 2014;371(26):2477-2487.
11. Wong TN, Miller CA, Jotte MRM, et al. Cellular stressors contribute to the expansion of hematopoietic clones of varying leukemic potential. *Nat Commun*. 2018;9(1):455.
12. Luna-Fineman S, Shannon KM, Lange BJ. Childhood monosomy 7: epidemiology, biology, and mechanistic implications. *Blood*. 1995;85(8):1985-1999.
13. Bejar R, Levine R, Ebert BL. Unraveling the molecular pathophysiology of myelodysplastic syndromes. *J Clin Oncol*. 2011;29(5):504-515.
14. Pezeshki A, Podder S, Kamel R, Corey SJ. Monosomy 7/del (7q) in inherited bone marrow failure syndromes: a systematic review. *Pediatr Blood Cancer*. 2017;64(12):e26714.
15. Luna-Fineman S, Shannon KM, Atwater SK, et al. Myelodysplastic and myeloproliferative disorders of childhood: a study of 167 patients. *Blood*. 1999;93(2):459-466.
16. Takahashi K, Wang F, Kantarjian H, et al. Copy number alterations detected as clonal hematopoiesis of indeterminate potential. *Blood Adv*. 2017;1(15):1031-1036.
17. Jacobs KB, Yeager M, Zhou W, et al. Detectable clonal mosaicism and its relationship to aging and cancer. *Nat Genet*. 2012;44(6):651-658.
18. Laurie CC, Laurie CA, Rice K, et al. Detectable clonal mosaicism from birth to old age and its relationship to cancer. *Nat Genet*. 2012;44(6):642-650.
19. Dimitriou M, Woll PS, Mortera-Blanco T, et al. Perturbed hematopoietic stem and progenitor cell hierarchy in myelodysplastic syndromes patients with monosomy 7 as the sole cytogenetic abnormality. *Oncotarget*. 2016;7(45):72685-72698.
20. An N, Khan S, Imgruet MK, et al. Gene dosage effect of CUX1 in a murine model disrupts HSC homeostasis and controls the severity and mortality of MDS. *Blood*. 2018;131(24):2682-2697.
21. McNerney ME, Brown CD, Wang X, et al. CUX1 is a haploinsufficient tumor suppressor gene on chromosome 7 frequently inactivated in acute myeloid leukemia. *Blood*. 2013;121(6):975-983.
22. McNerney ME, Brown CD, Peterson AL, et al. The spectrum of somatic mutations in high-risk acute myeloid leukaemia with -7/del(7q). *Br J Haematol*. 2014;166(4):550-556.
23. Zink F, Stacey SN, Norddahl GL, et al. Clonal hematopoiesis, with and without candidate driver mutations, is common in the elderly. *Blood*. 2017;130(6):742-752.
24. Yoshizato T, Dumitriu B, Hosokawa K, et al. Somatic mutations and clonal hematopoiesis in aplastic anemia. *N Engl J Med*. 2015;373(1):35-47.
25. Wong CC, Martincorena I, Rust AG, et al; Chronic Myeloid Disorders Working Group of the International Cancer Genome Consortium. Inactivating CUX1 mutations promote tumorigenesis. *Nat Genet*. 2014;46(1):33-38.
26. Aly M, Ramdzan ZM, Nagata Y, et al. Distinct clinical and biological implications of *CUX1* in myeloid neoplasms. *Blood Adv*. 2019;3(14):2164-2178.
27. Lindsley RC, Saber W, Mar BG, et al. Prognostic mutations in myelodysplastic syndrome after stem-cell transplantation. *N Engl J Med*. 2017;376(6):536-547.
28. Seguin L, Liot C, Mzali R, et al. CUX1 and E2F1 regulate coordinated expression of the mitotic complex genes Ect2, MgcRacGAP, and MKLP1 in S phase. *Mol Cell Biol*. 2009;29(2):570-581.
29. Ramdzan ZM, Nepveu A. CUX1, a haploinsufficient tumour suppressor gene overexpressed in advanced cancers. *Nat Rev Cancer*. 2014;14(10):673-682.
30. Li Q, Lau A, Morris TJ, Guo L, Fordyce CB, Stanley EF. A syntaxin 1, Galpha(o), and

N-type calcium channel complex at a presynaptic nerve terminal: analysis by quantitative immunocolocalization. *J Neurosci.* 2004;24(16):4070-4081.

31. Bolte S, Cordelières FP. A guided tour into subcellular colocalization analysis in light microscopy. *J Microsc.* 2006;224(Pt 3):213-232.

32. Ramdzan ZM, Ginjala V, Pinder JB, et al. The DNA repair function of CUX1 contributes to radioresistance. *Oncotarget.* 2017;8(12):19021-19038.

33. Mariotti LG, Pirovano G, Savage KI, et al. Use of the γ-H2AX assay to investigate DNA repair dynamics following multiple radiation exposures. *PLoS One.* 2013;8(11):e79541.

34. Vadnais C, Davoudi S, Afshin M, et al. CUX1 transcription factor is required for optimal ATM/ATR-mediated responses to DNA damage. *Nucleic Acids Res.* 2012;40(10):4483-4495.

35. Arthur RK, An N, Khan S, McNerney ME. The haploinsufficient tumor suppressor, CUX1, acts as an analog transcriptional regulator that controls target genes through distal enhancers that loop to target promoters. *Nucleic Acids Res.* 2017;45(11):6350-6361.

36. Nishio H, Walsh MJ. CCAAT displacement protein/cut homolog recruits G9a histone lysine methyltransferase to repress transcription. *Proc Natl Acad Sci USA.* 2004;101(31):11257-11262.

37. Shankar SR, Bahirvani AG, Rao VK, Bharathy N, Ow JR, Taneja R. G9a, a multipotent regulator of gene expression. *Epigenetics.* 2013;8(1):16-22.

38. Chaturvedi CP, Somasundaram B, Singh K, et al. Maintenance of gene silencing by the coordinate action of the H3K9 methyltransferase G9a/KMT1C and the H3K4 demethylase Jarid1a/KDM5A. *Proc Natl Acad Sci USA.* 2012;109(46):18845-18850.

39. Watanabe S, Iimori M, Chan DV, Hara E, Kitao H, Maehara Y. MDC1 methylation mediated by lysine methyltransferases EHMT1 and EHMT2 regulates active ATM accumulation flanking DNA damage sites. *Sci Rep.* 2018;8(1):10888.

40. Ginjala V, Rodriguez-Colon L, Ganguly B, et al. Protein-lysine methyltransferases G9a and GLP1 promote responses to DNA damage. *Sci Rep.* 2017;7(1):16613.

41. Yuan Z-F, Sidoli S, Marchione DM, et al. EpiProfile 2.0: a computational platform for processing Epi-proteomics mass spectrometry data. *J Proteome Res.* 2018;17(7):2533-2541.

42. Fnu S, Williamson EA, De Haro LP, et al. Methylation of histone H3 lysine 36 enhances DNA repair by nonhomologous end-joining. *Proc Natl Acad Sci USA.* 2011;108(2):540-545.

43. Ogiwara H, Ui A, Otsuka A, et al. Histone acetylation by CBP and p300 at double-strand break sites facilitates SWI/SNF chromatin remodeling and the recruitment of non-homologous end joining factors. *Oncogene.* 2011;30(18):2135-2146.

44. Yang Q, Zhu Q, Lu X, et al. G9a coordinates with the RPA complex to promote DNA damage repair and cell survival. *Proc Natl Acad Sci USA.* 2017;114(30):E6054-E6063.

45. Liu F, Barsyte-Lovejoy D, Li F, et al. Discovery of an in vivo chemical probe of the lysine methyltransferases G9a and GLP. *J Med Chem.* 2013;56(21):8931-8942.

46. Kondo Y, Shen L, Ahmed S, et al. Downregulation of histone H3 lysine 9 methyltransferase G9a induces centrosome disruption and chromosome instability in cancer cells. *PLoS One.* 2008;3(4):e2037.

47. Wu H, Chen X, Xiong J, et al. Histone methyltransferase G9a contributes to H3K27 methylation in vivo. *Cell Res.* 2011;21(2):365-367.

48. Tachibana M, Sugimoto K, Fukushima T, Shinkai Y. Set domain-containing protein, G9a, is a novel lysine-preferring mammalian histone methyltransferase with hyperactivity and specific selectivity to lysines 9 and 27 of histone H3. *J Biol Chem.* 2001;276(27):25309-25317.

49. Mozzetta C, Pontis J, Fritsch L, et al. The histone H3 lysine 9 methyltransferases G9a and GLP regulate polycomb repressive complex 2-mediated gene silencing. *Mol Cell.* 2014;53(2):277-289.

50. Zhang Y, Chang J-F, Sun J, et al. Histone H3K27 methylation modulates the dynamics of FANCD2 on chromatin to facilitate NHEJ and genome stability. *J Cell Sci.* 2018;131(12):jcs215525.

51. Ayrapetov MK, Gursoy-Yuzugullu O, Xu C, Xu Y, Price BD. DNA double-strand breaks promote methylation of histone H3 on lysine 9 and transient formation of repressive chromatin. *Proc Natl Acad Sci USA.* 2014;111(25):9169-9174.

52. Xu Y, Zhang S, Lin S, et al. WERAM: a database of writers, erasers and readers of histone acetylation and methylation in eukaryotes. *Nucleic Acids Res.* 2017;45(D1):D264-D270.

53. Lou Z, Minter-Dykhouse K, Franco S, et al. MDC1 maintains genomic stability by participating in the amplification of ATM-dependent DNA damage signals. *Mol Cell.* 2006;21(2):187-200.

54. Le Deley MC, Leblanc T, Shamsaldin A, et al; Société Française d'Oncologie Pédiatrique. Risk of secondary leukemia after a solid tumor in childhood according to the dose of epipodophyllotoxins and anthracyclines: a case-control study by the Société Française d'Oncologie Pédiatrique. *J Clin Oncol.* 2003;21(6):1074-1081.

55. Lu Y, Liu Y, Yang C. Evaluating in vitro DNA damage using comet assay. *J Vis Exp.* 2017;128(128):e56450.

56. Subramanian A, Tamayo P, Mootha VK, et al. Gene set enrichment analysis: a knowledge-based approach for interpreting genome-wide expression profiles. *Proc Natl Acad Sci USA.* 2005;102(43):15545-15550.

57. Bolton KL, Ptashkin RN, Gao T, et al. Cancer therapy shapes the fitness landscape of clonal hematopoiesis. *Nat Genet.* 2020;52(11):1219–1226.

58. Lu EP, McLellan M, Ding L, et al. Caspase-9 is required for normal hematopoietic development and protection from alkylator-induced DNA damage in mice. *Blood.* 2014;124(26):3887-3895.

59. Fenske TS, McMahon C, Edwin D, et al. Identification of candidate alkylator-induced cancer susceptibility genes by whole genome scanning in mice. *Cancer Res.* 2006;66(10):5029-5038.

60. Quwailid MM, Hugill A, Dear N, et al. A gene-driven ENU-based approach to generating an allelic series in any gene. *Mamm Genome.* 2004;15(8):585-591.

61. Wong TN, Ramsingh G, Young AL, et al. Role of TP53 mutations in the origin and evolution of therapy-related acute myeloid leukaemia. *Nature.* 2015;518(7540):552-555.

62. Gillis NK, Ball M, Zhang Q, et al. Clonal haemopoiesis and therapy-related myeloid malignancies in elderly patients: a proof-of-concept, case-control study. *Lancet Oncol.* 2017;18(1):112-121.

63. Kogan SC, Ward JM, Anver MR, et al; Hematopathology subcommittee of the Mouse Models of Human Cancers Consortium. Bethesda proposals for classification of nonlymphoid hematopoietic neoplasms in mice. *Blood.* 2002;100(1):238-245.

64. Lee WY, Weinberg OK, Pinkus GS. GATA1 is a sensitive and specific nuclear marker for erythroid and megakaryocytic lineages. *Am J Clin Pathol.* 2017;147(4):420-426.

65. Liu W, Hasserjian RP, Hu Y, et al. Pure erythroid leukemia: a reassessment of the entity using the 2008 World Health Organization classification. *Mod Pathol.* 2011;24(3):375-383.

66. Wong E, Ling V, Westerman D, Morgan S, Juneja S. How unique is pure erythroid leukaemia? A retrospective analysis of seven cases and review of the literature. *J Clin Pathol.* 2015;68(4):301-305.

67. Agarwal P, Jackson SP. G9a inhibition potentiates the anti-tumour activity of DNA double-strand break inducing agents by impairing DNA repair independent of p53 status. *Cancer Lett.* 2016;380(2):467-475.

68. Hosono N, Makishima H, Jerez A, et al. Recurrent genetic defects on chromosome 7q in myeloid neoplasms. *Leukemia.* 2014;28(6):1348-1351.

69. Shimizu T, Kubovcakova L, Nienhold R, et al. Loss of Ezh2 synergizes with JAK2-V617F in initiating myeloproliferative neoplasms and promoting myelofibrosis. *J Exp Med.* 2016;213(8):1479-1496.

70. Churpek JE, Marquez R, Neistadt B, et al. Inherited mutations in cancer susceptibility genes are common among survivors of breast cancer who develop therapy-related leukemia. *Cancer.* 2016;122(2):304-311.

71. Schulz E, Valentin A, Ulz P, et al. Germline mutations in the DNA damage response genes BRCA1, BRCA2, BARD1 and TP53 in patients with therapy related myeloid neoplasms. *J Med Genet.* 2012;49(7):422-428.

72. Bhatia S. Genetic variation as a modifier of association between therapeutic exposure and subsequent malignant neoplasms in cancer survivors. *Cancer*. 2015;121(5):648-663.

73. Voso MT, Fabiani E, Zang Z, et al. Fanconi anemia gene variants in therapy-related myeloid neoplasms [letter]. *Blood Cancer J*. 2015;5(7):e323.

74. Marusyk A, Porter CC, Zaberezhnyy V, DeGregori J. Irradiation selects for p53-deficient hematopoietic progenitors. *PLoS Biol*. 2010;8(3):e1000324.

75. Prokocimer M, Molchadsky A, Rotter V. Dysfunctional diversity of p53 proteins in adult acute myeloid leukemia: projections on diagnostic workup and therapy. *Blood*. 2017; 130(6):699-712.

76. Stoddart A, Fernald AA, Wang J, et al. Haploinsufficiency of del(5q) genes, Egr1 and Apc, cooperate with Tp53 loss to induce acute myeloid leukemia in mice. *Blood*. 2014; 123(7):1069-1078.

77. Mitsumori K, Onodera H, Shimo T, et al. Rapid induction of uterine tumors with p53 point mutations in heterozygous p53-deficient CBA mice given a single intraperitoneal administration of N-ethyl-N-nitrosourea. *Carcinogenesis*. 2000;21(5):1039-1042.

78. Harvey M, McArthur MJ, Montgomery CA Jr, Butel JS, Bradley A, Donehower LA. Spontaneous and carcinogen-induced tumorigenesis in p53-deficient mice. *Nat Genet*. 1993;5(3):225-229.

79. van de Haar J, Canisius S, Yu MK, Voest EE, Wessels LFA, Ideker T. Identifying epistasis in cancer genomes: a delicate affair. *Cell*. 2019; 177(6):1375-1383.

80. Park Y, Gerson SL. DNA repair defects in stem cell function and aging. *Annu Rev Med*. 2005; 56:495-508.

81. Rossi DJ, Bryder D, Seita J, Nussenzweig A, Hoeijmakers J, Weissman IL. Deficiencies in DNA damage repair limit the function of haematopoietic stem cells with age. *Nature*. 2007;447(7145):725-729.

82. Sedelnikova OA, Horikawa I, Zimonjic DB, Popescu NC, Bonner WM, Barrett JC. Senescing human cells and ageing mice accumulate DNA lesions with unrepairable double-strand breaks. *Nat Cell Biol*. 2004;6(2):168-170.

83. Popp HD, Naumann N, Brendel S, et al. Increase of DNA damage and alteration of the DNA damage response in myelodysplastic syndromes and acute myeloid leukemias. *Leuk Res*. 2017;57:112-118.

84. Sun D, Luo M, Jeong M, et al. Epigenomic profiling of young and aged HSCs reveals concerted changes during aging that reinforce self-renewal. *Cell Stem Cell*. 2014; 14(5):673-688.

85. Adelman ER, Huang HT, Roisman A, et al. Aging human hematopoietic stem cells manifest profound epigenetic reprogramming of enhancers that may predispose to leukemia. *Cancer Discov*. 2019;9(8):1080-1101.

86. Appelbaum FR, Gundacker H, Head DR, et al. Age and acute myeloid leukemia. *Blood*. 2006;107(9):3481-3485.

87. Edgar R, Domrachev M, Lash AE. Gene Expression Omnibus: NCBI gene expression and hybridization array data repository. *Nucleic Acids Res*. 2002;30(1):207-210.

88. AACR Project GENIE Consortium; Sweeney SM, Cerami E, Baras A, et al. AACR project GENIE: powering precision medicine through an international consortium. *Cancer Discov*. 2017;7(8):818-831. >Human Tissue Resource Center (RRID:SCR_019199),